ACT/ICAPS - Thermoplastic Composite Activities

M. P. Renieri, S. J. Burpo, L. M. Roundy
and S. M. Todd

McDonnell Aircraft Company
St. Louis, Missouri

SUMMARY

McDonnell Aircraft Company (MCAIR) is teamed with Douglas Aircraft Company (DAC) under NASA's Advanced Composites Technology (ACT) initiative in a program entitled Innovative Composite Aircraft Primary Structures (ICAPS). Efforts at MCAIR have focused on the use of thermoplastic composite materials in the development of structural details associated with an advanced fighter fuselage section with applicability to transport design.

Based on innovative design/manufacturing concepts for the fuselage section primary structure, elements were designed, fabricated and structurally tested. These elements focused on key issues such as thick composite lugs and low cost forming of fastenerless, stiffener/moldline concepts. Manufacturing techniques included autoclave consolidation, single diaphragm co-consolidation (SDCC) and roll-forming.

INTRODUCTION

A major obstacle to widespread use of high performance composites in primary aircraft structures is the high cost of manufacture and assembly. Under NASA's ACT program, McDonnell Aircraft Company investigated cost-effective innovative techniques for the fabrication and joining of primary airframe structure using thermoplastic composite materials. While these developments were directed toward an Advanced Short Take-off or Vertical Landing (ASTOVL) aircraft, they are equally applicable to commercial vehicle structure. Efforts in these programs were conducted in design and structural mechanics development, manufacturing concepts development, and structural testing. Due to NASA program redirection, efforts were curtailed at the element level. This report summarizes progress through element verification. The elements addressed key design issues associated with the fuselage section; fastenerless frame attachment concepts, thick composite lugs, and rolled-formed stiffeners.

Structural verification testing was performed on the element specimens. Pull-off strength tests at ambient and elevated-temperature-wet conditions were conducted on the fastenerless frame concepts. To assess analytical developments, thick lug tests were performed under ambient conditions for two lug geometries and three laminate configurations.

GENERIC FUSELAGE SECTION

The advanced aircraft system selected for the fighter development effort was the Model 4629 ASTOVL design developed by MCAIR under the NASA-Ames sponsored U.S./U.K. ASTOVL Technology Development program. Based on representative fuselage cross-sections of the Model 4629 aircraft, a generic center fuselage structure, Figure 1, was developed as the primary structure demonstration component. While the fuselage structure contains design features particular to advanced ASTOVL aircraft, cost-effective fabrication techniques and innovative design concepts developed in this program demonstrated technology related to all emerging aircraft systems.

MATERIAL AND PROCESS SELECTIONS

Material

The material chosen was based on temperature requirements, solvent resistance, component design, manufacturing approaches, and processing ease. Due to the 255°F design requirement, the baseline thermoplastic resin system selected was ITX (intermediate temperature crystalline), which has service capability to 300°F. ITX processing temperature and pressure ranges are 700°-750°F and 100-150 psi, respectively, as such processing characteristics are similar to ICI's APC-2 (PEEK) system. Amorphous systems were not considered due to their poor resistance to solvents such as jet fuel.

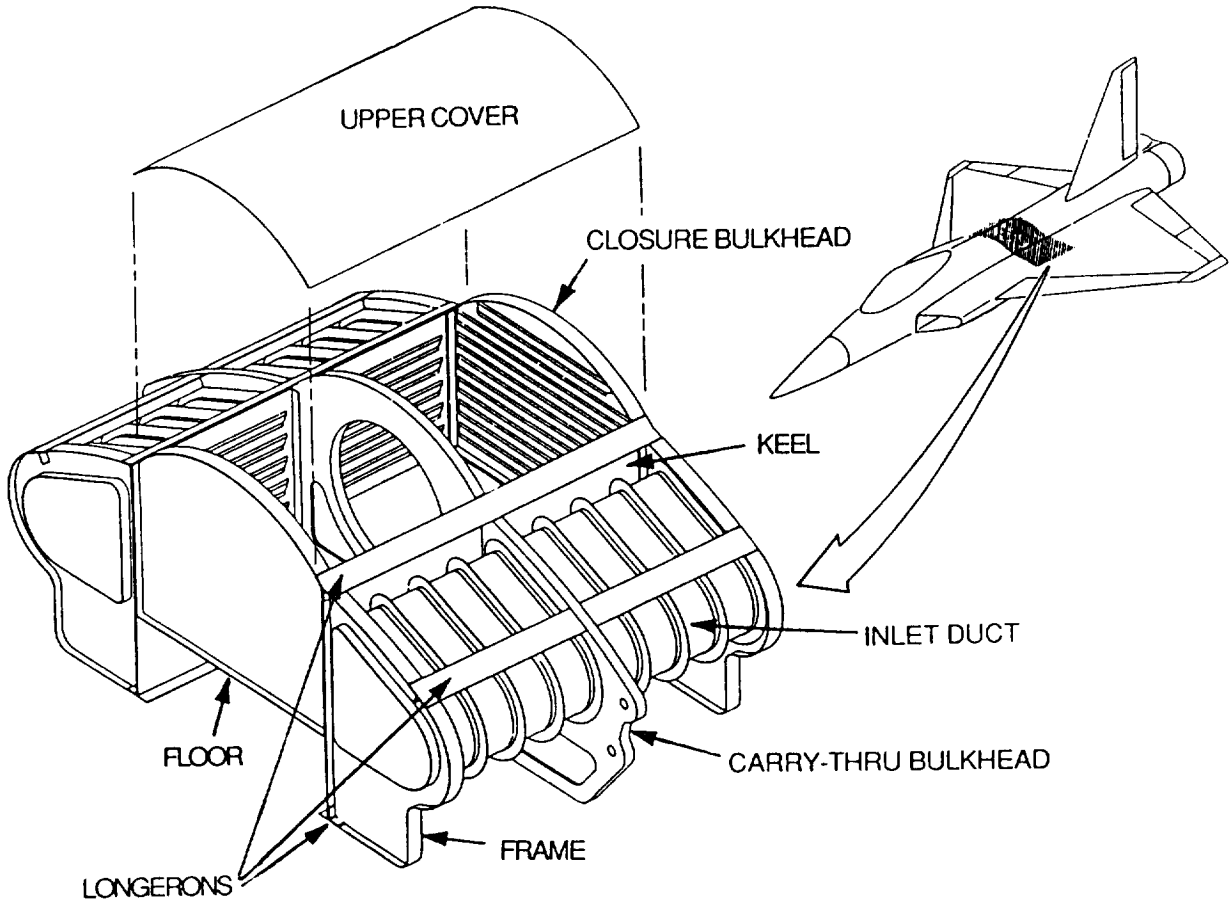

Figure 1 Generic Fuselage Section Offered a Full Range of Design and Manufacturing Challenges

The fiber selected was IM7, an intermediate modulus fiber produced by Hercules. In addition, AS4/APC-2 was selected for early forming studies due to immediate availability and to verify analytical predictions for thick composite lugs.

Processes

Manufacturing processes were selected using a concurrent engineering approach. Processes were rated based on innovativeness, cost, risk, supportability, survivability, and weight. Two manufacturing techniques, fiber placement and single diaphragm/coconsolidation (SDCC), were determined to be potential low cost fabrication techniques (Reference 1).

Fiber placement (FP), one of the more promising methods of fabrication, is the in-situ consolidation of individual material layers using pressure and heat at the point of contact. This procedure eliminates the autoclave requirement and automates the material deposition process reducing significant cost elements in a typical composite production environment. Work using this approach area was discontinued due to program redirection.

Single diaphragm/coconsolidation (SDCC) simultaneously consolidates the hat stiffened inner skin plies with the outer skin plies while coconsolidating the two yielding a high quality interface and reducing the number of process steps from three to one. This approach was used to fabricate representative fastenerless frame attachment concepts developed in this program.

SDCC Manufacturing Concept

The SDCC concept is unique in that there is but one diaphragm, and the IML pan and OML skin are coconsolidated during the diaphragm forming process. The SDCC tooling concept is illustrated in Figure 2. A vacuum frame is utilized to hold the IML ply pack prior to heat-up and pressurization. The greatest risk in diaphragm forming over hat mandrels is the chance for bridging. To reduce this risk, hat spacing is minimized to increase ply surface area between mandrels. The increased surface area increases the forces exerted to form the ply pack and prevent bridging. In addition, the mandrels are fabricated with a slight radius, Figure 3. The gap between the mandrel, OML skin and IML pan are filled with a predetermined amount of unidirectional tow. This fillet area has the highest probability for bridging; however, with the unidirectional fillet, the pressure would be equally distributed to facilitate a quality consolidation.

A vacuum ring and a neat film layer aid in ply pack location. The IML ply pack is contained between the aluminum diaphragm and a layer of neat film. A vacuum ring surrounds the IML ply pack and vacuum draws the aluminum diaphragm to the upper surface of the IML ply pack, and the neat film to the lower surface of the IML ply pack. The IML ply pack is then positioned above the tool prior to application of heat and pressure. The neat film is coconsolidated between the IML and OML ply packs during the press operation. This permits accurate location of the IML ply pack and aids in the prevention of wrinkles.

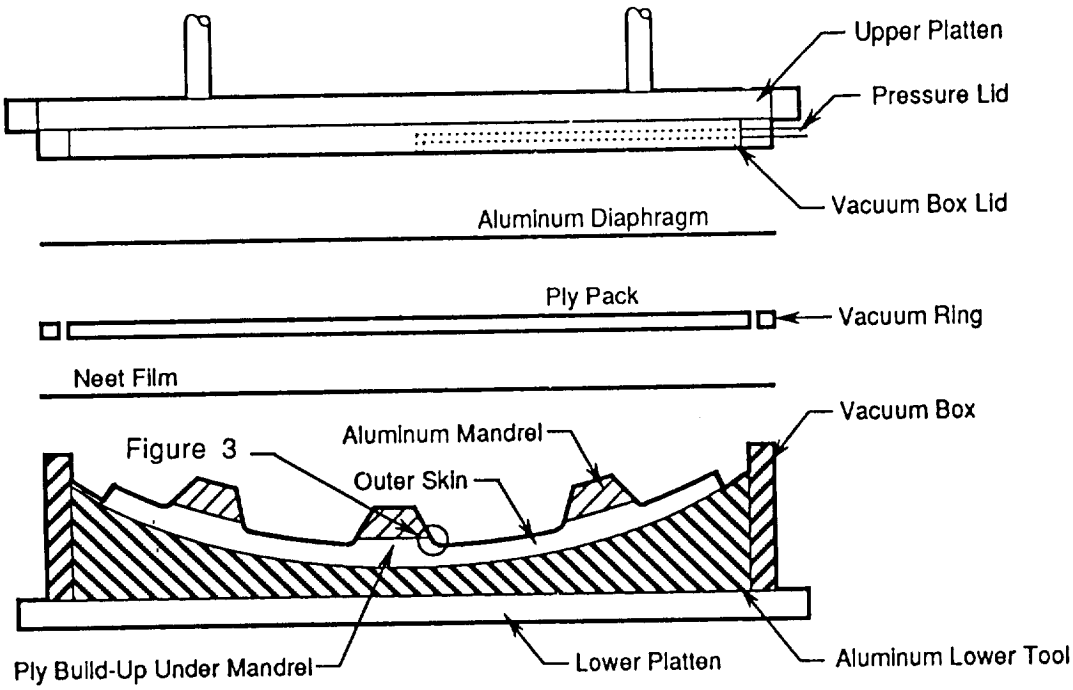

Figure 2 Single Diaphragm Coconsolidation (SDCC) Concept Offered Potential for Low Cost Manufacturing

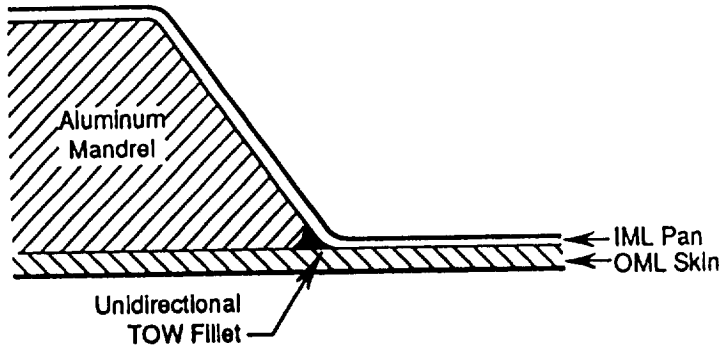

Figure 3 Unidirectional Tow Used in Fillet Area to Assure Part Quality

THERMOPLASTIC FUSELAGE ELEMENT CONCEPTS

As a first phase to the building block approach to the production of a full-scale fighter fuselage section, element components were selected for design, analysis, and structural validation. Element selections were sought which would address key areas of the innovative composite design including structural design, analysis, and manufacturing development. In addition, the elements were to be representative of key components within the future phases of the subcomponent development.

Two structural areas of particular interest in the fuselage structure were identified by the Design/Manufacturing Integration (D/MI) team. Stiffener to skin joints were selected based upon:

- anticipated increases in performance through optimal design for pull-off and shear-transfer loading
- decreased costs through manufacturing innovations such as the SDCC approach
- potential for LO applications, reduced weight, and reduced assembly due to the fastenerless design associated with SDCC
- current MCAIR developments for the analysis of stiffener pull-off strengths and comparative test data

Thick composite lugs were identified as the second element for evaluation based upon:

- anticipated increases in performance through optimal design for pin-bending effects and through-the-thickness loading effects
- decreased costs through the validation of water-jet-cutting of thick composites for initial and final trim
- current developments in thick composite analysis which could be enhanced to provide a useful design/analysis tool for the evaluation of highly loaded and out-of-plane loading of thick composites

Frame Elements

Frame Element Design - A fastenerless moldline Y-frame attachment design was selected due to its applicability to the diaphragm forming coconsolidation technique. The design was also anticipated to generate substantially greater strengths for pull-off and shear transfer due to the increased interlaminar shear and tension strengths associated with semicrystalline thermoplastic composites. The design therefore exploited both the mechanical and manufacturing strengths of the thermoplastic material system.

The Y-frame layup consisted of identical outer-moldline (OML) and Y-section (IML) laminates [+45/90/0/90/+45]. The inner and outer skin was to be coconsolidated during the diaphragm forming process. The only design variable was the attachment angle of the two Y-frame legs. This geometric parameter controls the ratio of shear to flat-wise tension loading at the frame/skin interface. In order to establish a better understanding of both the material allowables, failure modes, and failure locations, two (2) geometries were chosen. A 45° and 60° angle of incidence was established based upon initial parametric evaluations. Although initial analysis was unable to show a distinct difference in failure mode for these two geometries it did identify differences in the failures loads associated with each. The finalized designs incorporating the SDCC manufacturing method and the differing leg angles are shown in Figure 4.

In order to establish a baseline comparison, blade elements were also designed and analyzed. The blade configuration, Figure 5, incorporates back-to-back angle laminates which are identical in layup to the Y-section legs. The OML skin was chosen to be equivalent to the "bay skin" used in the Y-section, [+45/90/0/90/+45]s. This design yields a substantially stiffer skin section beneath the frame attachment, but was chosen in order to maintain the critical stacking sequence in the corner radius and provide an identical skin laminate in the area of applied constraints for the testing procedure.

SDCC Y-Frame Elements Fabrication - An SDCC element verification tool, Figure 6, was developed which incorporated either two hat mandrels or a single triangular mandrel to simulate fabrication of stiffener and frame designs, respectively. The entire tool was located in a vacuum forming box to facilitate the SDCC manufacturing process.

The verification tool was first utilized as a parallel hat-section tool to verify stiffener fabrication. The hat stiffener mandrels, located by pins, float on the unconsolidated skin. The inner skin was then formed over the mandrels in a press operation. A pinning arrangement allows the mandrels to float during consolidation. These pins permit the consolidation force to be transferred through the mandrels to the part to insure a quality consolidation. The aluminum tools were readily extracted following forming.

Due to program redirection, hat-section forming trials were discontinued and attention concentrated on forming of the Y-frame elements. Lessons learned from the hat-section trials were incorporated into this effort. To minimize diaphragm rupture due to sharp corners, the tooling was modified by extending the mandrels to the ramps of the forming box, Figure 7. In addition, application of full pressure should take place after the plies have reached melt temperature instead of just before melt. This allows the matrix to reach its minimum viscosity before forming is initiated. Previously, pressure was introduced prior to melt temperature to encourage interply slippage between the upper and lower ply packs. Due to the bridging observed on the room temperature forming trials, it was decided that forming depth would be improved if the ply pack was at full melt temperature.

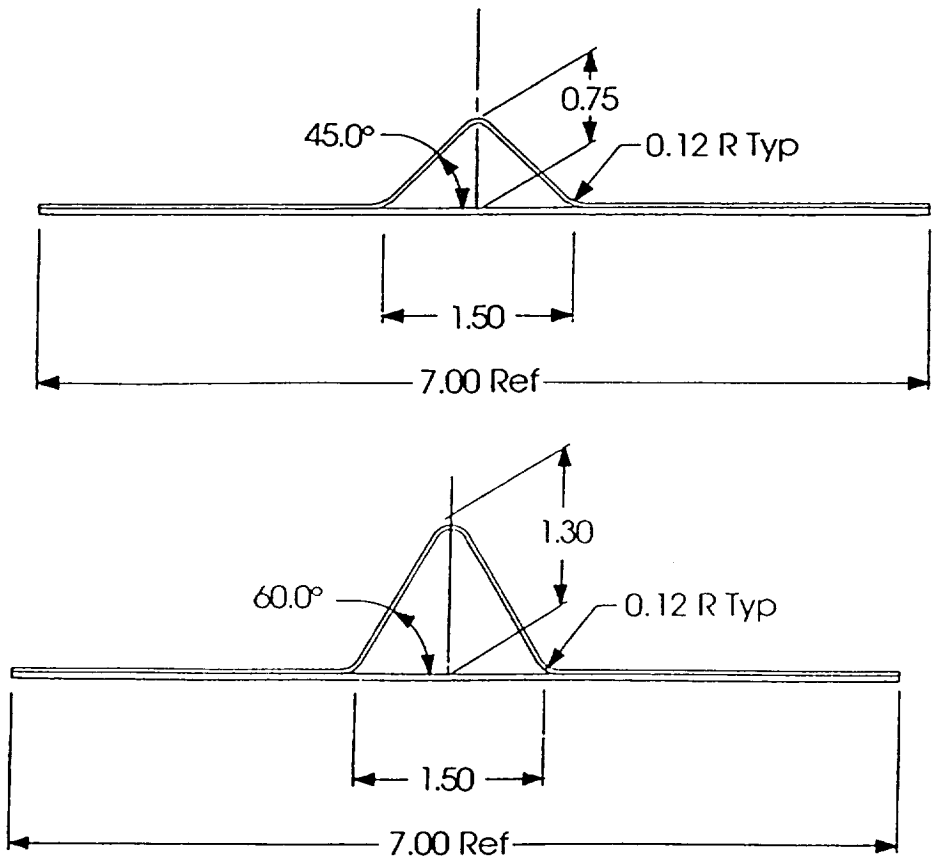

Figure 4 SDCC Y-Frame Element Designs Used to Determine Viability of Fastenerless Attachment Concepts

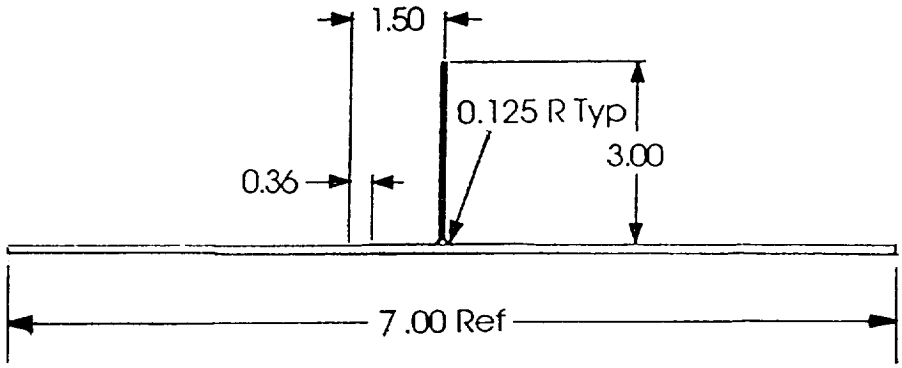

Figure 5 Blade-Frame Element Design Used for Baseline

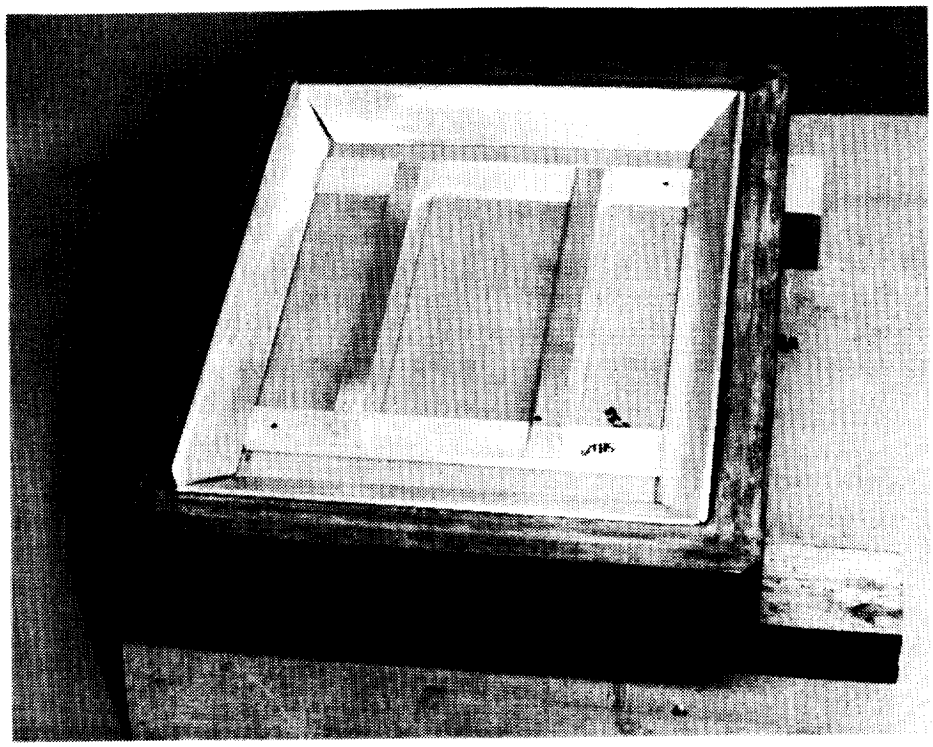

Figure 6 SDCC Element Verification Tool Incorporated Full Scale Design Features

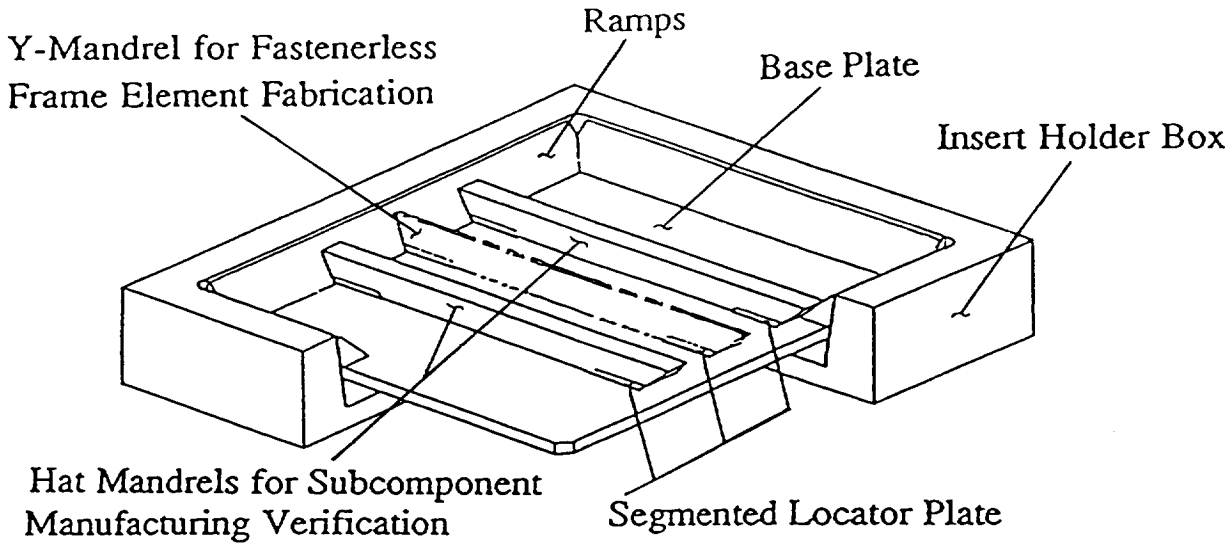

Figure 7 Modifications to SDCC Element Verification Tool Eliminated Early Diaphragm Ruptures (Segmented Locator Plates and Mandrel Extension)

Forming trials on the single "Y" configuration used one diaphragm to consolidate the upper ply pack with the lower plies. Initially, full pressure (150 psi) was applied after the melt temperature of the ITX was reached, but was maintained for only 5 minutes at which point the diaphragm ruptured. In spite of the short hold time the pressure was sufficient to fully consolidate the flat areas of the part and to form the material over the mandrel. The upper ply pack conformed to the mandrel surface, but diaphragm rupture caused the outer ply to lift and bridge across the mandrel/skin intersection. The other plies remained in the formed condition, nesting closely to the mandrel and showed an excellent definition at the interface between stiffener web and lower skin.

Forming was next done below melt temperature because of anticipated problems where the two ply packs met each other beyond the stiffener area. For the next trial full melt temperature was achieved before pressurizing. The upper ply pack was also widened so it extended out to the ramps in all directions. This change required notches to be cut along the edge of the ply pack so it wouldn't buckle and rupture the diaphragm. Kapton tape was used to cover the notches for additional protection.

Forming trials were performed with the above changes and the diaphragm survived fairly well up through 150 psi. Since the plies were well melted by this time, relatively good consolidation was achieved between the upper and lower packs. Rupture occurred along the edge of the mandrel in a notch location that allowed the film to over elongate. A large percent of the plies remained formed to the mandrel surface along its base. Only one ply lifted and bridged away from the radius area of the formed plies, Figure 8. The inside of the stiffener shape revealed very good contact between the plies being formed and the base of the mandrel even with loss of the diaphragm. Photomicrographs of the area revealed the upper plies dragged the lower plies in toward the mandrel and formed wrinkles in the lower skin.

In an attempt to alleviate dragging of the base ply pack, the upper ply of the base pack was extended to run under the ramp areas of the tool. This change would maintain pressure on the top ply to allow slippage of the two ply packs without wrinkling. Also, a fiber glass cloth (picture frame) was placed around the ramp areas and over the mandrel to cover any areas that could potentially allow the diaphragm to rupture. An additional change to the process was to initiate application of the forming pressure at 600°F. The rationale was to apply pressure below melt-temperature of the material to allow ply slippage prior to a viscosity change. During this run the diaphragm ruptured in a gap between the ramp and forming box causing incomplete forming of the element. However, improved ply slippage was noted due to the reduced temperature.

Due to the frequency of rupture of the UPILEX diaphragms, an aluminum (SUPRAL) diaphragm was selected for further trials. The aluminum diaphragm offered greater elongation capabilities not only at processing temperatures, but also at temperatures below the melt temperature of the PEEK resin.

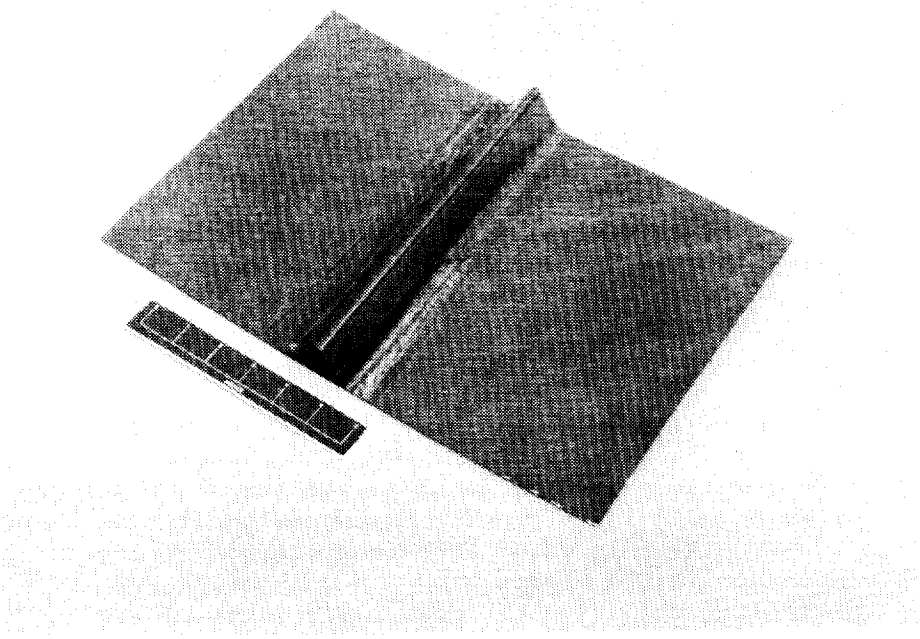

Figure 8 Initial SDCC Y-Frame Element Experienced Bridging in Radius

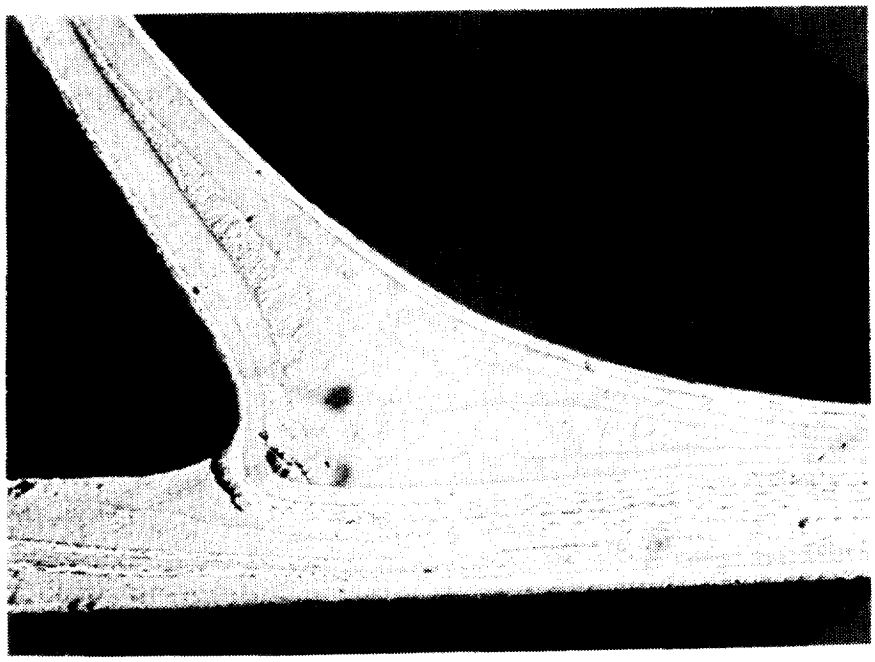

Figure 9 Ply Wrinkling Occurred in SDCC Y-Frame Corner Radius During One-Step Forming

During the first run with an aluminum diaphragm, the pressure was applied at 550°F. Applying the pressure at this low temperature allowed for additional ply slippage prior a viscosity change of the resin. During this fabrication attempt, the top ply of the lower ply pack was extended beneath the forming ramps in an attempt to "lock" the ply in place, thus avoiding wrinkles. After applying pressure (120 psi) at 550°F, the temperature was increased to 750°F and held for 30 minutes.

The result was a stiffened panel with good surface quality but bridging in the radius. NDE results revealed a porosity free part in the flat areas. However, photomicrographs revealed the lower ply pack wrinkled. Since the upper ply of the lower ply pack wrinkled, and the ends were contained beneath the forming ramps, the ply obviously split between the fibers of this outer 45° ply.

Following review of the results of the run, two changes to the manufacturing process were identified to alleviate the wrinkling problem in the next run. First a .003" layer of neat resin was applied to the bondline to serve as lubricant. The film would allow the two contacting plies to slip past each other and form in the radius area. A photomicrograph of the radius area following processing utilizing the neat resin is presented in Figure 9. As can be seen, radius cracking and bridging are present along with wrinkling in the lower ply pack. 0° plies were then added at the interface to allow the inner and outer ply packs to more readily slip past one another. The results revealed similar problems as noted with the neat resin.

To overcome friction between the two surfaces, it was decided that the upper ply pack should be driven into the radius areas prior to reaching the glass transition temperature. This would allow the plies to slip past one another prior to a viscosity change. To accomplish this, the upper ply pack was preconsolidated and then coconsolidated to the lower ply pack in a second operation. With this approach the risk level is significantly reduced while maintaining a major processing cost reduction.

The 45° and 60° Y-stiffened element panels were fabricated successfully using the two-step process as typified in Figures 10 and 11. The upper ply pack was preconsolidated utilizing the diaphragm forming process. Following consolidation, the upper ply pack was coconsolidated to the lower ply pack. Although this is a change from the original SCDD concept, a cost savings is still realized by reducing the process to two steps from a traditional three-step process.

The 45° and 50° Y-stiffener panels were nondestructively evaluated. The C-scan results on the 60° panel showed a quality part free of voids. The 45° Y-stiffened panel, however, revealed slight porosity under the mandrel. This was due to a piece of sheet metal slipping beneath the mandrel during consolidation. The sheet metal was modified and another 45° panel fabricated with excellent results from NDE.

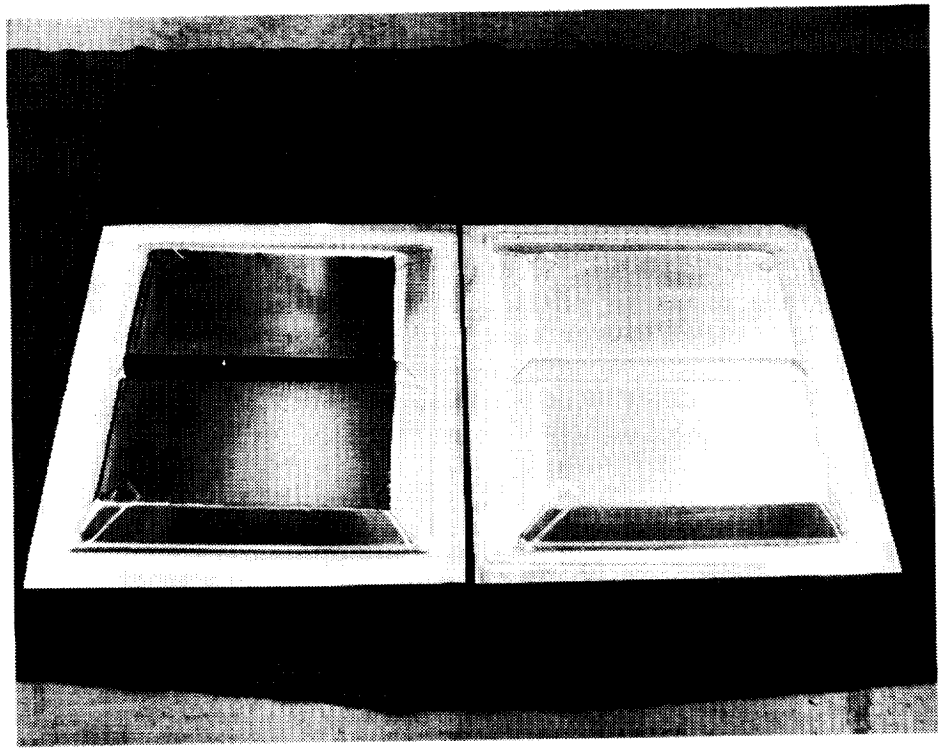

Figure 10 Aluminum Diaphragms and Two-Step Forming Provided Quality Y-Frame Elements

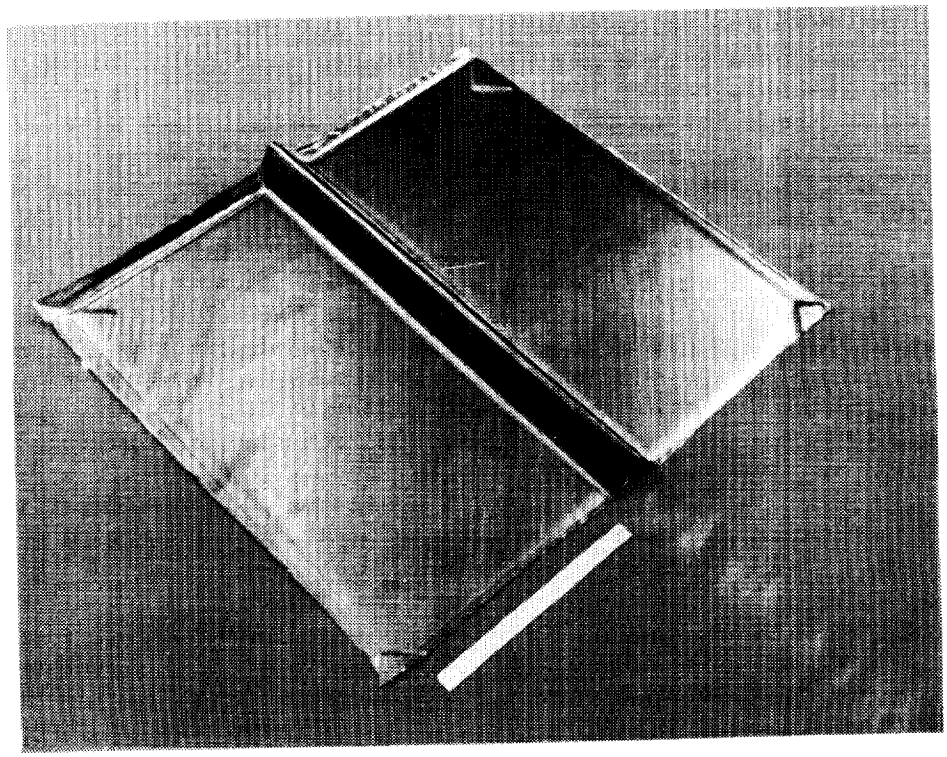

Figure 11 Typical Two-Step Diaphragm Formed 60° Y-Frame Element

The dual-step SDCC process reflects a significant cost reduction compared to conventional diaphragm forming of integrally stiffened skin structure which involves a three-step approach; forming of the inner corrugated skin, forming of the outer skin, and subsequent coconsolidation. In addition, the three-step process involves the use of an additional diaphragm for outer skin forming.

Our original intent was to develop a single-step SDCC process. Our attempts were unsuccessful due primarily to dragging of outer moldline skin plies into corner radii of the corrugations during forming of the inner moldline skin. The dual-step process was then adopted to insure timely fabrication of the element test specimens.

Blade Frame Elements Fabrication - Using two aluminum block details a blade panel was hand laminated by bending and edge tacking each of seven plies with a soldering iron, Figure 12. The fillet was filled with thin strips (.30" to .90") of ITX unidirectional tape using a sharp cone tip on the soldering iron. A flat skin was preconsolidated and a strip grit blasted across the center where the blade attached, Figure 13. The two angles with fillet in place were inverted onto this skin, Figure 14, and vacuum bagged to a project plate. There was a released UPILEX film between the angle plies (web) and the aluminum details. Upon consolidation, at 750°F and 100 psi, the part did not show acceptable C-scan results. The web area had many depressions in it that appeared to be oriented along the second ply down from the surface, i.e., normal to the surface ply fiber direction.

Outgassing from the release coated UPILEX and the lack of ears on the vacuum bag at the base (which may have prevented sliding of the blocks) were identified as probable causes for the poor consolidation. As such, a second blade was fabricated with no UPILEX on the tool details and with extensive ear folds in the vacuum bag. Nondestructive inspection of the second blade revealed porosity in the radius areas. Although the part quality was improved over the first blade, it was not the level desired. One of the tool details had rotated during consolidation causing poor consolidation in the web and radius areas.

The consolidation tools were then modified to permit a positive control of the details. A trimetric view of the modification is shown in Figure 15. Keyways were milled into the ends of the web details and fit to guides in the end plates. This modification maintained the movement of the detail in the direction desired thus maintaining constant and equal pressure across the part surfaces. In addition, an upper slotted plate maintained minimum differential vertical displacement between the tooling blocks for the back-to-back L-section which comprises the T-section.

The modified tooling concept is a positive drive concept designed to maintain cap and web thickness while providing adequate pressure on the part. Conventional forming tools utilize mechanical stops to provide constant web and cap thickness. However, mechanical stops can contact the project plate prematurely reducing pressure on the part and ultimately causing porosity.

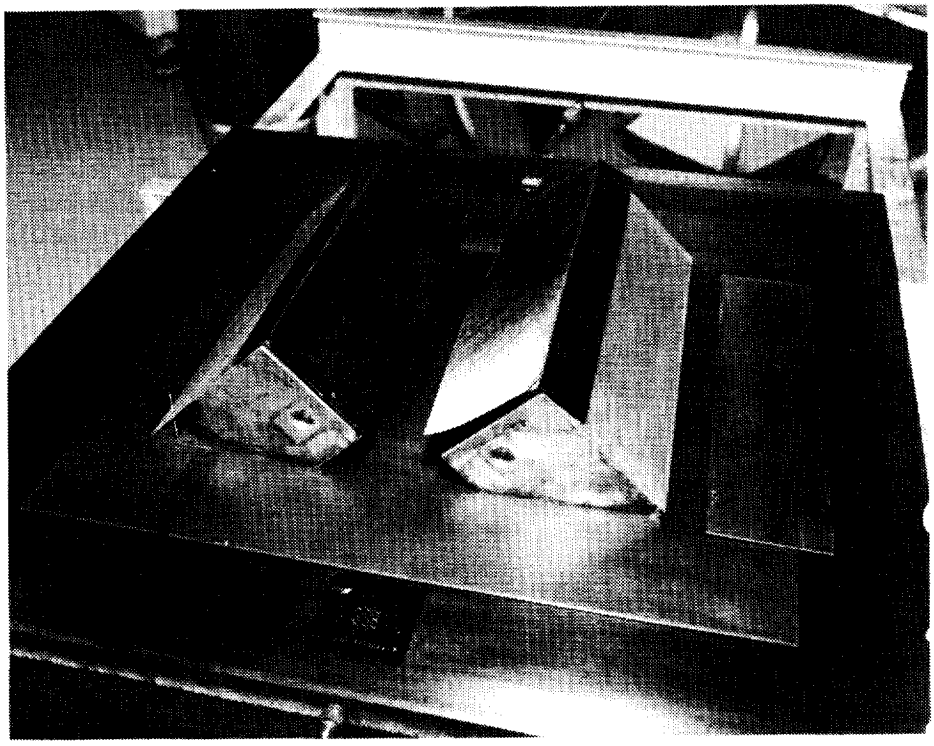

Figure 12 Blade L-Section Plies were Formed on Tooling Blocks to Form Web

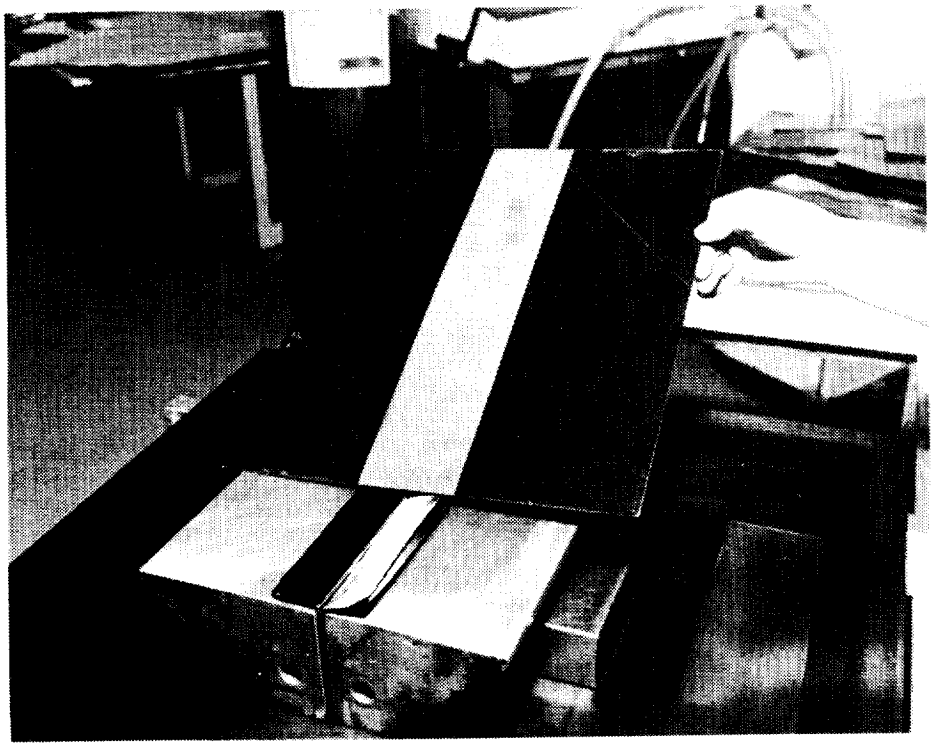

Figure 13 Base Plies were Consolidated Separately and Grit Blasted Prior to Assembly

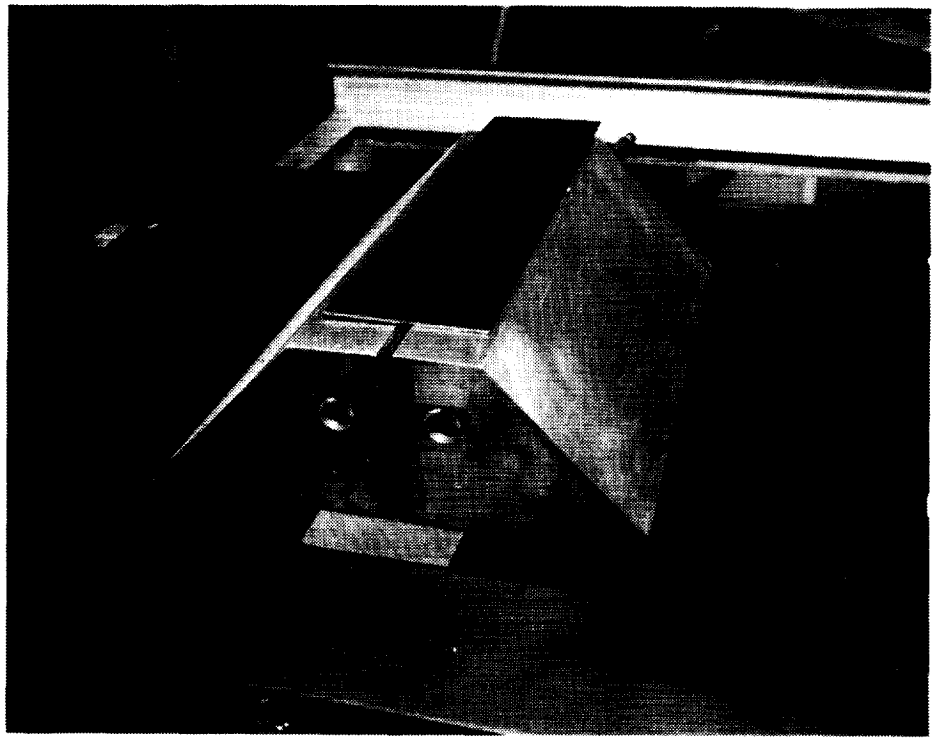

Figure 14 Blade Laminate/Tooling Assembly Prior to Autoclave Consolidation

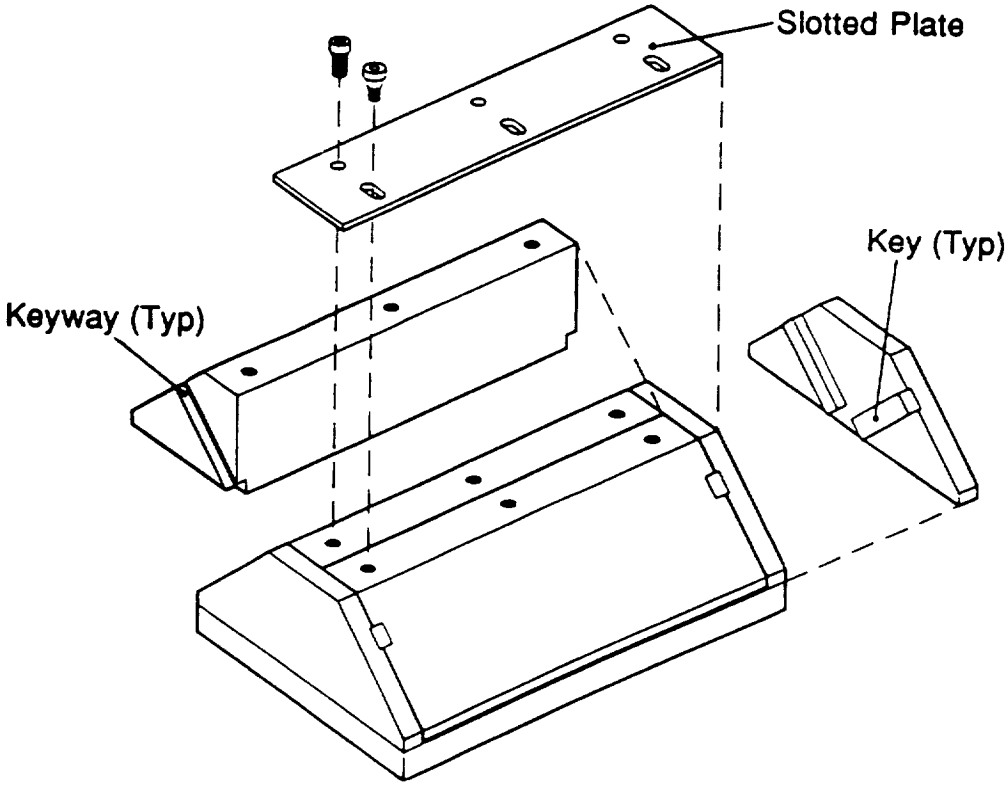

Figure 15 Modification to Blade Element Tooling Provided Necessary Pressure on Web and Radius

Using the same lay-up approach previously described and the positive drive tooling concept, a quality part was achieved on the first attempt, Figure 16. However, due to amount of fillet material used, a slight void was noted in a photomicrograph of the radius area. Following review of the photomicrograph, it was concluded that excessive 0° tow was being used in the fillet, and that the dwell time should be increased. During a second run, the two changes were incorporated in the consolidation process. The element was then C-scanned revealing a quality consolidation. Photomicrographs show total consolidation in the fillet area as well as the cap and web. A thickness check of the cap and web show only a .001" variation. This element panel was cut into specimens for pull-off testing, Figure 17.

A blade panel previously consolidated with the original tooling concept and exhibiting unacceptable levels of porosity was reconsolidated using the positive drive tooling. Both C-scan and photomicrographic inspections revealed a quality part. This blade element was also machined into element specimens in order to investigate the effects of reconsolidation. It is worthy to note that this latter scenario demonstrates potential cost savings associated with the ability to reconsolidate thermoplastic composites.

Frame Element Tests - Frame element testing was conducted on the fastenerless frame attachment designs which were selected for subcomponent and full-scale development. In addition, testing was conducted on an induction welded frame concept in order to initially assess the feasibility of this joining method for later use under the full-scale development.

Nondestructive Evaluation (NDE) revealed some minor porosity and defects in the 45° Y-specimen panel. An additional panel was fabricated to provide specimens. With the exception of induction welded Y-frame specimens, all coconsolidated specimens were determined to be of good quality. Difficulty in the examination of the corner radii was experienced for all specimens. Based upon available C-scan data and examination of the specimens after final trimming all specimens were accepted.

A dimensional check was conducted to further verify the accuracy of fabrication of all specimens and to establish a database for later failure correlation. The results of the dimensional checks showed minor variations (less than 10% deviation from nominal) in thicknesses and specimen widths. The width dimension was utilized to normalize all reported load data to pounds per unit width.

All specimen configurations were subjected to two (2) testing conditions as shown in Figure 18. Room temperature dry (RTD) testing was conducted on specimens which underwent an initial weighing followed by exposure to 250°F until weight loss stabilized. Elevated temperature wet (ETW) test specimens experienced the same 250°F drying exposure followed by moisture conditioning at 160°F and 95% RH. Based on a time history of the moisture conditioning, an average equilibrium moisture content for the IM7/ITX frame element was found to be 0.34% by weight.

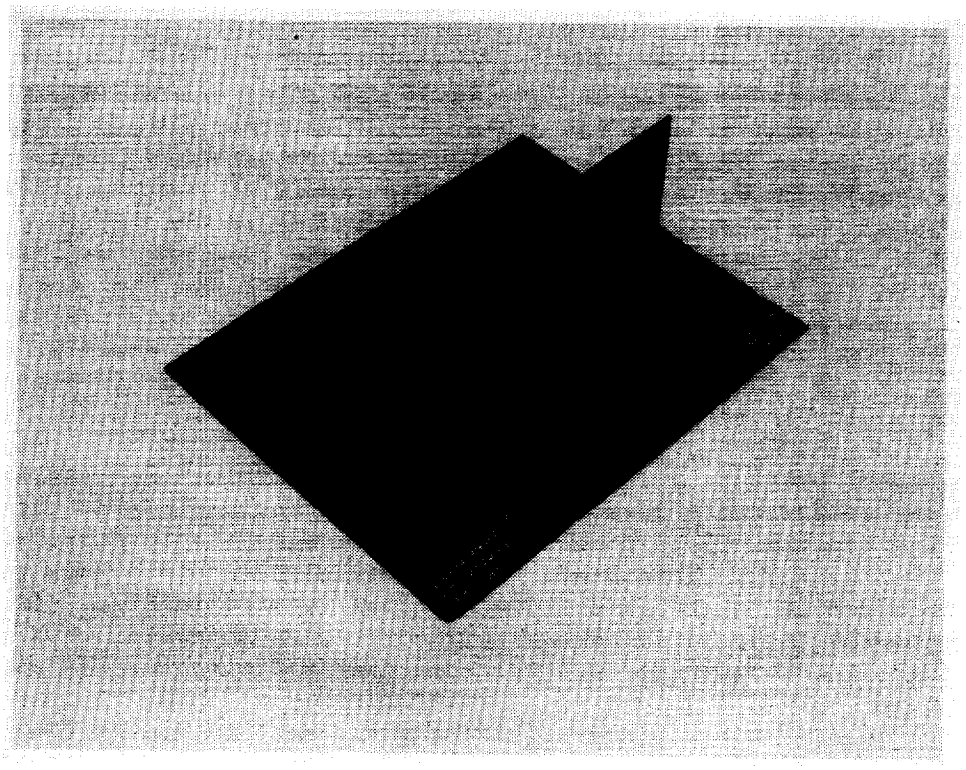

Figure 16 Typical Blade Frame Element

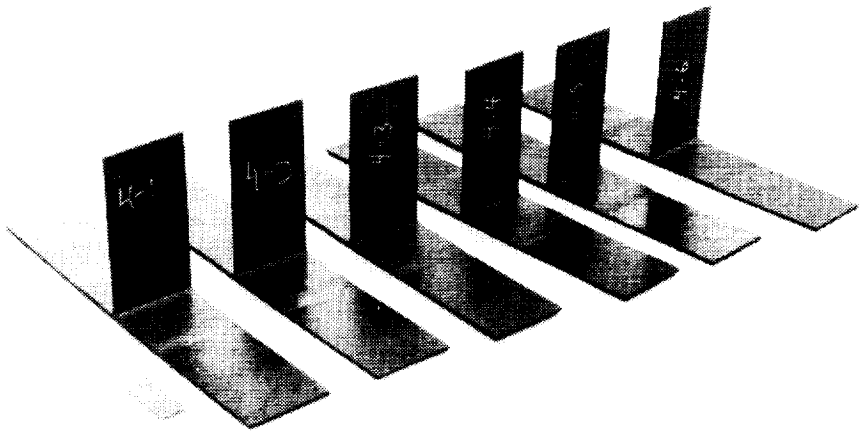

Figure 17 Blade Frame Element Panels were Machined into Pull-Off Specimens

Frame Configuration	Fabrication Process	Number of Specimens at Test Environment	
		RTD*	ETW**
Blade	Co-Consolidated	3	3
45° Y-Frame	Co-Consolidated	3	3
60° Y-Frame	Co-Consolidated	3	3

Figure 18 Fastenerless Frame Element Testing Matrix Used to Demonstrate Increases in Pull-Off Strengths

The test setup for room temperature specimens is shown in Figure 19 for both the baseline blade and Y-frame specimens. Load introduction for the blade specimens was accomplished through direct gripping of the upstanding flange. A loading mandrel and clevis were utilized for the Y-frames. Initial testing showed substantial deflections due to the 5" span used between end clamps. In order to eliminate excessive deflections the test procedure was modified to provide a 3" span. The identical setup was used for the elevated temperature testing, with the test apparatus enclosed within a temperature control chamber. A thermocouple was utilized to ensure accurate control of the temperature to the required 250°F. A hold time of 5 minutes was utilized to ensure temperature uniformity for the part while reducing the risk of desorption associated with longer hold times.

Testing was carried out utilizing a displacement control rate of 0.1 in/min. Load versus deflection plots were obtained for each test condition. In addition to on-line recording of the load history, continuous visual inspection of the specimens was carried out during testing in order to establish initial failure modes and a correlation to the loading data. Videotaping of the initial room temperature tests provided a means of reviewing the test procedures (including load and displacement histories monitored on digital readouts). In addition, specimen edges were painted white prior to testing in order to provide contrast and enhance visual identification of failure initiation and location.

A summary of test results is presented in Figures 20 and 21. The following sections provide a detailed discussion of each of the specimen groups that were examined under element testing. A final overview and discussion of results follow these sections.

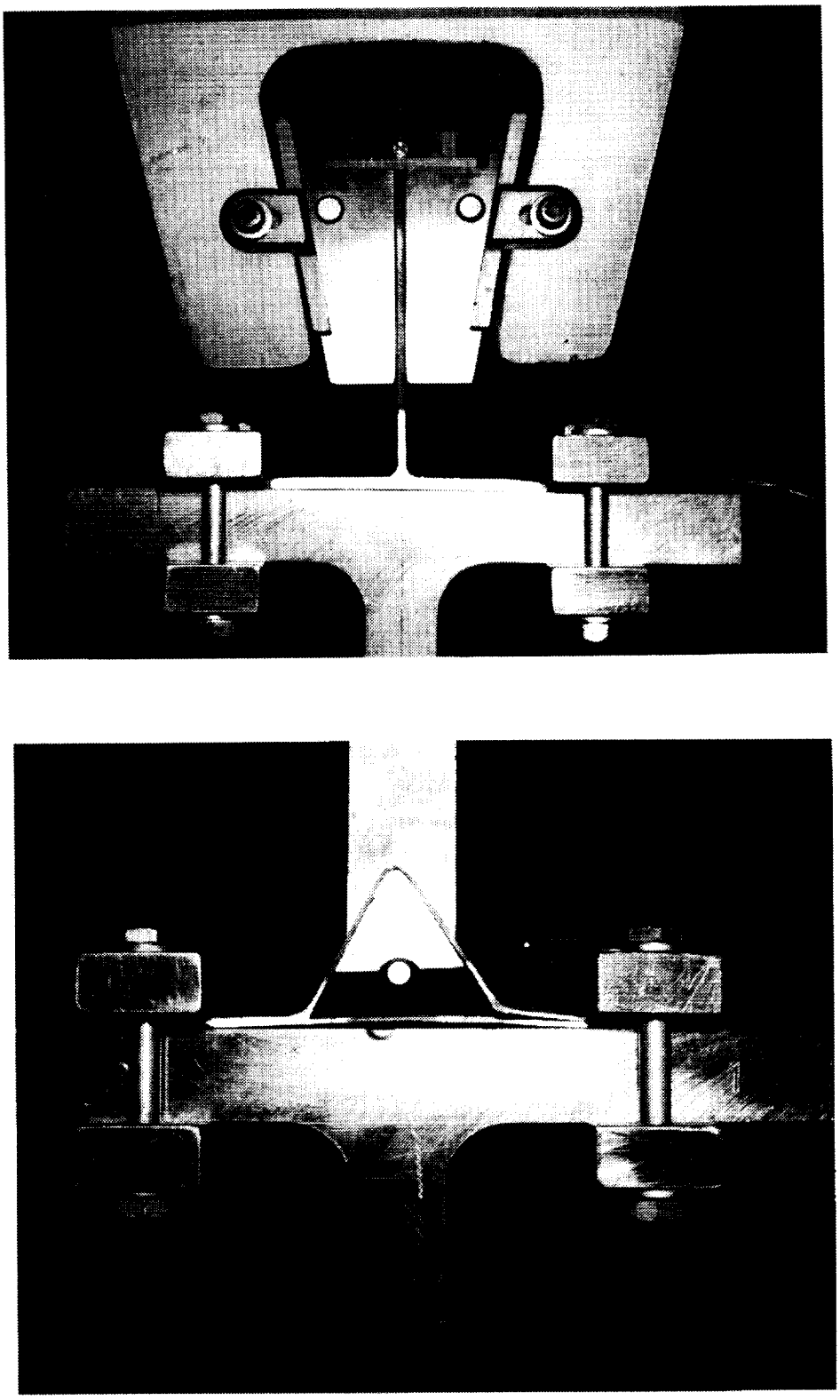

Figure 19 Typical Frame Element Pull-Off Test Set-Up

Frame Configuration	Initial Failure			Final Failure		
	Load (lbs/in)	Deflection (in)	Failure Mode	Load (lbs/in)	Deflection (in)	Failure Mode
Blade	328	0.124	ILT Failure* at Corner	315	0.178	Interface Failure**
45° Y-Frame	554	0.148	Skin Surface Failure at Clamp	655	0.216	ILT + Interface Failure
60° Y-Frame	504	0.161	Skin Surface Failure at Clamp	574	0.247	ILT + Interface Failure

* Interlaminar Tension Failure at Frame Corner
** Interface Failure between Base Skin and Flange

Figure 20 Y-Frame Designs Demonstrated Significant Increase in Pull-Off Strength (RTD Tests)

Frame Configuration	Initial Failure			Final Failure		
	Load (lbs/in)	Deflection (in)	Failure Mode	Load (lbs/in)	Deflection (in)	Failure Mode
Blade	372	0.155	Comp. Failure in Lower Skin	417	0.255	Interface Failure*
45° Y-Frame	530	0.145	Skin Surface Failure at Clamp	746	0.270	Interface Failure
60° Y-Frame	—	—	—	615	0.192	Interface Failure

* Interface Failure between Base Skin and Flange

Figure 21 Y-Frame Designs Demonstrated Significant Increase in Pull-Off Strength (ETW Tests)

RTD Blades - Each of the RTD blade specimens exhibited a distinctive initial failure which was associated with a radius crack within the angle ply pack. This initial failure was visually observable and correlated exactly with initial load drop-off. Propagation of the initial crack continued through the remainder of the loading sequence. A second failure was observed to correspond to the loss of the bond between the skin and frame laminates as the radius crack progressed to the interface. The final portion of the load/ displacement curve indicated the continued loss of the interface as a result of the crack propagation with the second failure load of lower magnitude than the crack initiation load. Cracks associated with initial and final failure are readily observable for a typical failed specimen shown in Figure 22.

RTD 60° Y- Frames - Initial failures in the Y-frames were associated with compression failure of the skin laminates at the clamped boundary condition. This failure is the cause of the decreased section stiffness and resulted without any indication of interface failures. Final failures typically occurred after a slight increase in load and substantially larger deflections.

Increases in the final failure load for a Y-frame element over the blade configuration are a result of decreased interlaminar tension stresses through redistribution of the pull-off load into combined interlaminar tension (ILT)

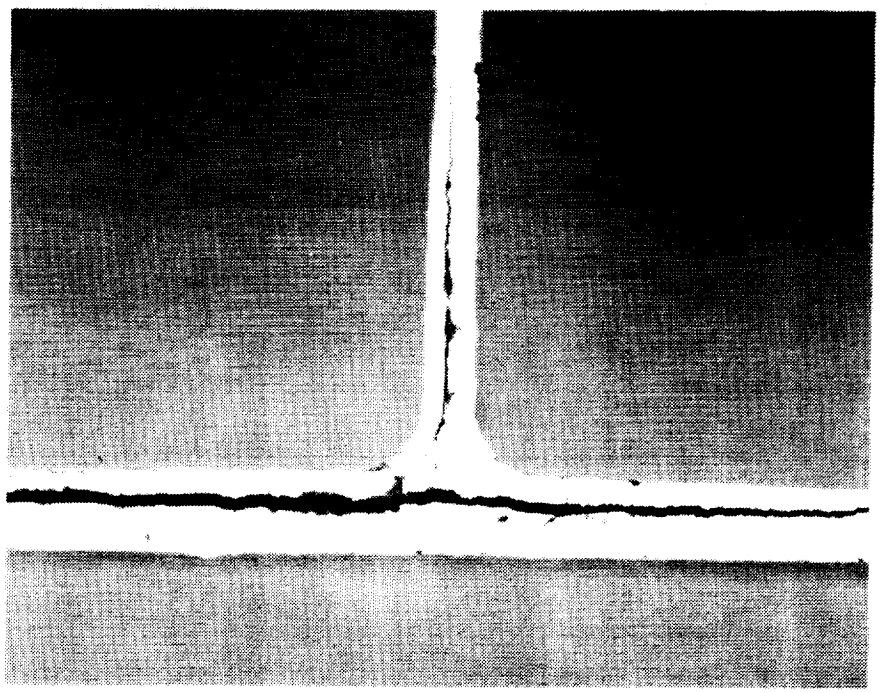

Figure 22 RTD Blade Elements Experienced Skin/Flange Interface Separation

and interlaminar sheal (ILS). In addition, ILT stress within the upstanding flange laminates is reduced due to the increased radius associated with this geometry. Observation of the final failure for the 60° element, Figure 23, showed crack initiation occurred as a result of interlaminar tension within the IML skin and resulted in catastrophic failure of the section.

RTD 45° Y-Frames - Nearly identical specimen response as observed for the 60° element was observed for the 45° geometry. This similarity includes initial non-linearity, minor variations due to slip, initial failure due to skin compression and associated reduction in modulus, and substantially higher ultimate pull-off strength. However, the 45° elements all showed continued load carrying capacity following the secondary ILT failure. This additional loading is more pronounced than any observed in the 60° elements and is associated with geometry and load redistribution effects. The larger open angle of the IML skin and further increase in corner radius decreases the ILT stresses within the IML laminate. In addition, loading continues to be redistributed into predominantly ILS stresses, as in the 60° frame. Failure observation for the 45° element showed crack initiation occurred as a result of ILT within the IML skin as previously witnessed in the 60° specimens. However, final failure eventually resulted from propagation of this crack to the interface and continuation of this delamination primarily through a shear mechanism. This crack growth proceeded at a slower rate than observed for either of the previous designs.

ETW Blades - Failure of the blade specimens became a more complicated phenomena for the elevated temperature wet condition. A higher degree of non-linearity in the initial load/displacement curve was recorded. Initial failures occurred as the result of compression in the lower skin. Both of these results are attributed to the softening of the material associated with the ETW condition. Very shortly after initial failure, a secondary failure in the interface was observed. Crack initiation occurred at the identical location as for the RT tests. Following crack initiation, secondary failure load carrying capacity of the frame attachment continued beyond the initial failure loads. Crack propagation was observed to progress far more slowly due to the plastitization of the matrix material. Eventual loss of all strength was associated with the loss of a significant portion of the flange to skin interface (approximately 50%).

Failure loads for all of the blade specimens considerably higher than the RTD tests. Similar results for lap shear specimens have been reported in previous work conducted at MCAIR. The mechanism for this increase in ETW strength is identical for both test situations. Elevated temperature response for the interface material shows a decrease in both stiffness and strength. However, an associated increase in ultimate strain is associated with the material due to its plastic response. The lap shear data has shown that the associated energy that the material is capable of absorbing prior to failure is significantly increased due to the large plastic deformations that become possible for the ETW material. The effect of the plasticity is to lower the peak stresses at the ends of interfaces while increasing the stresses across the remainder of the interface. This results in an increase in the total load

carrying capacity of the interface. The plasticity also accounts for the non-linearity observed during the initial portion of the load/displacement plot.

ETW 60° Y-Frames - The 60° frame elements exhibited the same degree of non-linearity that was observed for the blade specimens. Skin compression failures occurred at the clamp location but to a much lesser extent than previously encountered for RT testing. No indication of skin compression failures beneath the frame attachment point was evident during the test or in the load/deflection history. A typical failed specimen is shown in Figure 24. Failure at the IML to OML interface occurred with immediate propagation of this failure to the clamp locations. No failures were witnessed within the IML skin due to interlaminar tension as observed in the RTD testing.

The increase in ultimate loading over the baseline blade configuration was also observed for these specimens and again indicates the advantage of redistributing load into ILS and ILT through the Y-frame design.

ETW 45° Y-Frames - Failure of the 45° frame specimens was more severe than had been witnessed in the 60° frame specimens and is attributed to the increased deflection observed in these specimens. Compression skin failure occurred at the clamped boundary. Final failure again occurred with the total failure of the interface due to primarily shear loading. The full failure of the interface is another indication that the plasticity of the matrix material is allowing the entire interface to carry more load than in the room temperature cases. This increased plastic loading prohibits the interface from resisting any cracks which initiate.

Overview of Frame Element Tests - Testing of the fastenerless frame attachments provided the necessary experience with these designs to allow for risk reduction in future scale up to subcomponent and full-scale articles. Of primary importance has been the demonstration of significant increases in the pull-off strength of frame attachments that can be achieved through Y-section designs. Through the examination of two geometries an initial understanding of the effects of geometry on load redistribution and strength improvements has been gained. Gains on the order of 50% were achieved for designs involving a 60° frame element as compared to the baseline blade. An additional improvement of 10% was obtained when the interior angle of the Y-section was reduced to 45°. These improvements are based upon initial failure loads for all of these sections and are summarized in Figure 25. Increases in section deflections were also evident in the test data. This fact points out the importance of including a local pad-up beneath the Y-section for future design developments.

Elevated temperature testing demonstrated the improvements in performance associated with a thermoplastic material subjected to interlaminar shear and tension. These increases are justified when considering the potential for plastic deformation of the matrix material in the interface. Some concern over this type of response will undoubtedly remain until an understanding of the possible fatigue response is investigated.

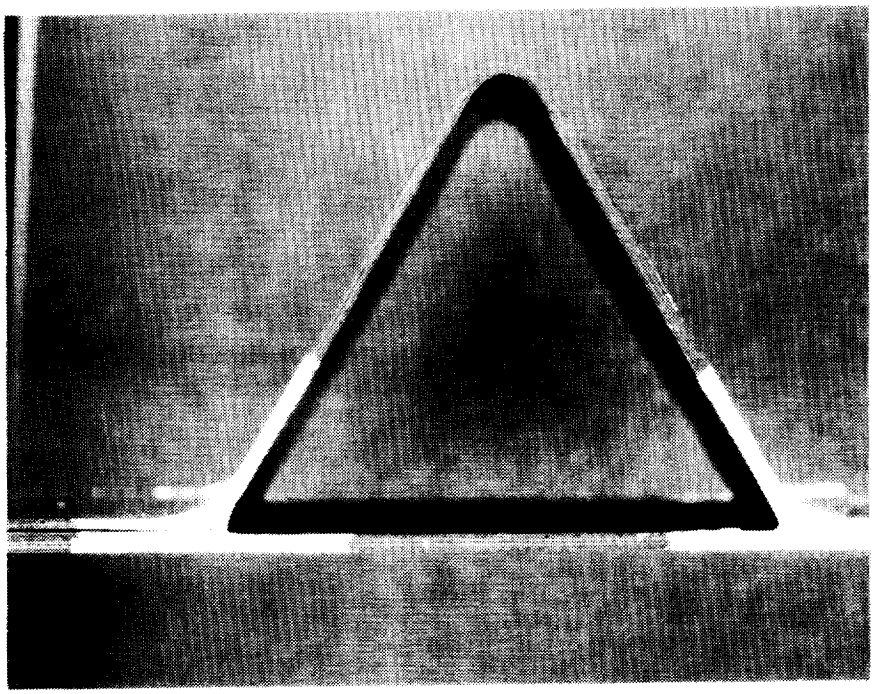

Figure 23 RTD 60° Y-Frame Elements Experienced Skin/Flange Interface Separation and Interlaminar Tension Failures

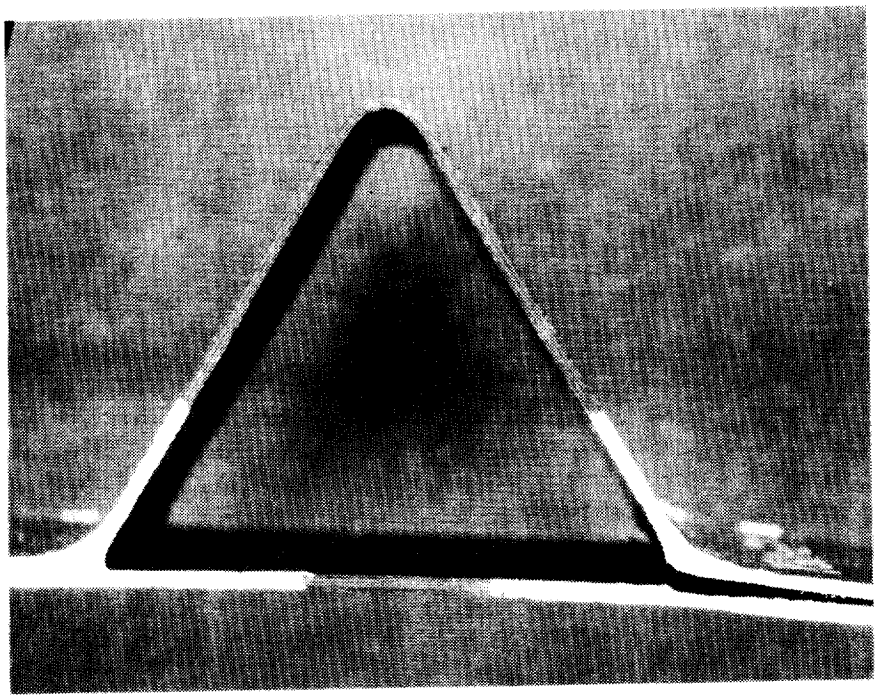

Figure 24 ETW 60° Y-Frame Elements Experienced Skin/Flange Interface Separation

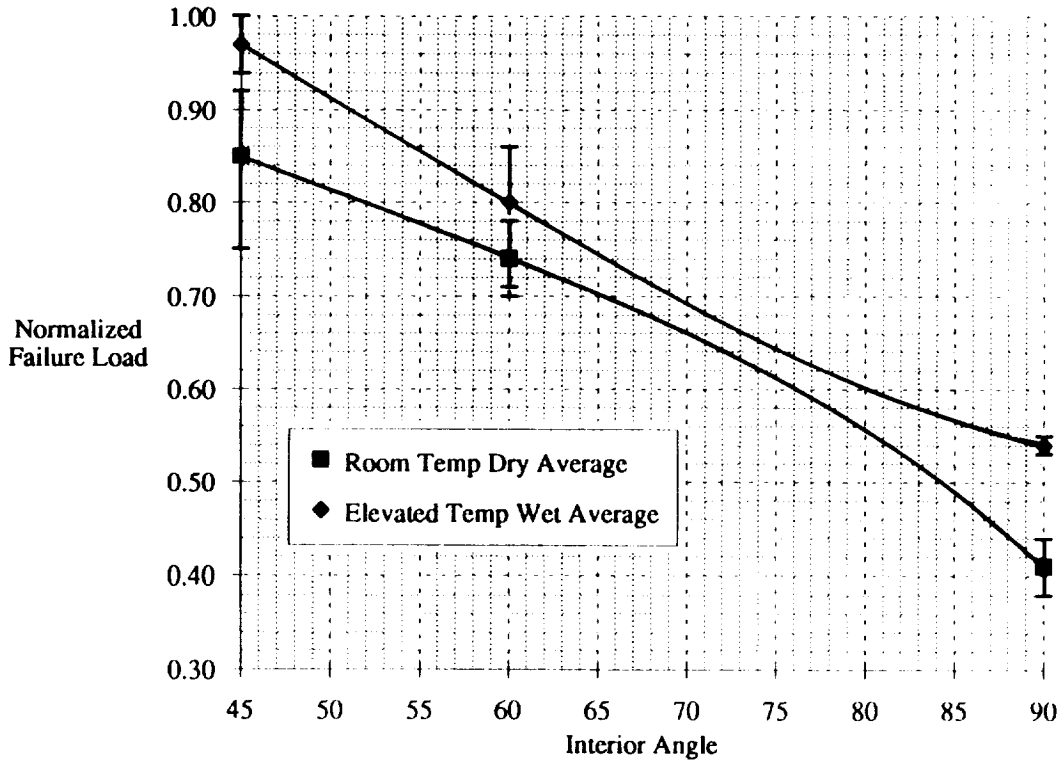

Figure 25 Performance Improvements Associated with Y-Frame Designs

With regard to testing, it is evident that future attempts must identify a means of load introduction which will not produce an interference between the load mechanism and the lower skin section. It is also recommended that skin thicknesses be increased to prohibit bending failures at the grip locations. These changes to the base laminate should include the addition of the previously mentioned pad-up region beneath the Y-section. A means of eliminating slipping beneath the clamping device should be found. As an alternative, the use of simple (or rollered) supports might be examined. This problem might also be advantageously influenced by the increased skin thickness already proposed. Finally, it should be mentioned that the use of videotaping in conjunction with the use of white-out on the specimen edges proved to be invaluable in correlating test results with observed failure modes.

Lug Elements

Lug Element Designs - In aircraft design, single-pinned joints (i.e., lugs) play a key role in the transmission of large loads between major structural components. Thus, the potential for substantial weight reductions exists in the use of composite materials for these highly loaded structures.

Unlike most element design efforts, the design of lug elements was not focused on identifying an optimal design for application to the fuselage structure and loading being considered. Instead, the designs were chosen to provide a fairly comprehensive set of test cases to which analytical developments could be compared. This form of building block approach was adopted due to the complexities involved in the design of both lugs and thick composite sections. The end result would be an analysis package with the means of rapidly comparing multiple design strategies later as the definition of the full-scale article became solidified.

The design of thermoplastic lug test articles focused on providing specimens which could validate the most critical portions of the analysis. Pin bending effects and a study of the different failure modes were targeted by the D/MI team as the primary areas of concern. A means of separating these design variables and maintaining constancy for all other design parameters became the focus of the team.

Previous in-house efforts determined that ply stacking sequences can affect the pin bending response of a lug. By varying the through-the-thickness stiffness distribution of the laminate, peak stresses could be reduced, thereby minimizing pin bending effects. In order to explore this potential for increased performance and to validate the methodology's ability to predict it, three lug layups were chosen which resulted in different pin bending responses while maintaining nearly identical in-plane response. This was accomplished by varying the stacking sequence of the six sublaminates used in the manufacture of each lug. Maintaining the in-plane response was necessary to allow for an investigation of the other design parameter, failure mode.

Failure mode dependence on lug geometry is well established for metallic designs and was anticipated to be the case for the composite lugs also. Lug geometries were chosen to provide two distinct modes of failure based on a metallic analysis using smeared in-plane properties for the composite lugs. External geometries on all the lugs were held constant (W = 3.5"), while the hole diameter was varied to 1.0" or 1.75". This resulted in different W/D ratios (3.5 and 2.0 respectively), and was anticipated to provide bearing failures in 50% of the specimens, while the remainder would experience net-section failures. A summary of the lug designs used for analysis correlation is shown in Figure 26 and represents the approach for exploration of critical design issues in composite lug analysis.

The analysis development pursued under this program was originally reported in Reference 2 and reported in more detail in a subject paper at this conference.

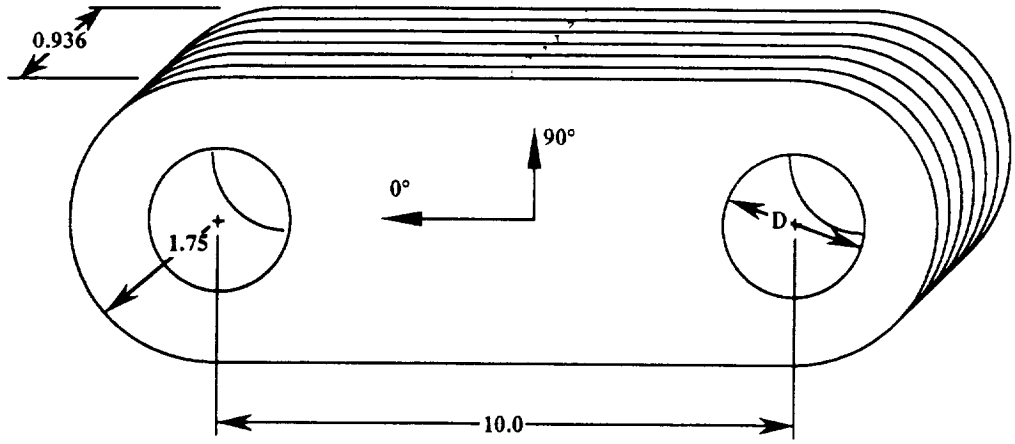

Note : All dimensions are inches.

Lug Specimens	Quantity	Hole Diameter (in)	Sublaminate Stacking Distribution*			Effective Layup
			Sublaminate 1	Sublaminate 2	Sublaminate 3	
Static 1	4	1.00	(47/40/13)	(47/40/13)	(47/40/13)	(47/40/13)
Static 2	3	1.00	(47/40/13)	(34/53/13)	(60/27/13)	(47/40/13)
Static 3	4	1.00	(60/27/13)	(47/40/13)	(20/67/13)	(42/45/13)
Static 4	4	1.75	(47/40/13)	(47/40/13)	(47/40/13)	(47/40/13)
Static 5	4	1.75	(47/40/13)	(34/53/13)	(60/27/13)	(47/40/13)
Static 6	4	1.75	(60/27/13)	(47/40/13)	(20/67/13)	(42/45/13)

* Sublaminate Stacking Sequences are as follows:

(47/40/13) : $[0_2/45_2/90_2/-45_2/0_2/45/0/-45/0_2]s$

(34/53/13) : $[45_2/0_2/-45_2/90_2/45_2/0_2/-45_2/0]s$

(60/27/13) : $[0_2/45/0_2/-45/0_2/45/0_2/-45/90_2/0]s$

(20/67/13) : $[45_2/0/-45_2/90/45_2/0/-45_2/90/45/0/-45]s$

Figure 26 Configuration and Stacking Sequence of Lug Elements Used to Verify Analytical Developments

Lug Element Fabrication - The lugs were fabricated using AS4/APC-2 unidirectional tape since it was readily available early in the program and the lugs were primarily being tested for analytical model verification. Tooling for the lug specimens consisted of simple project plates with steel plates positioned to allow for expansion during consolidation.

The lugs were fabricated from eighteen 30" x 16" sublaminate panels of four different 30 ply lay-ups. The sublaminates were consolidated in a hydraulic press. Six sublaminates were stacked to form the three different 180 ply stacking sequences which were coconsolidated in the autoclave. Excellent consolidation of the sublaminates was verified by photomicrograph inspection. Panels with the final lug lay-ups were C-scanned to ensure their quality.

Water jet cutting was used to obtain four lugs from each of the panels, Figure 27. The finish associated with this cutting procedure was acceptable as the final external finish on the test articles. Initial lugs showed a minor defect on the external surface at the beginning of the radius. This was associated with the initiation of the WJC process and to avoid this stress riser, the cutting pattern was altered to begin in the middle of the lug rather than at a radius.

The pin holes were initially WJC and secondarily milled to ensure the necessary tolerances of $\pm$.005 inches. C-scans were taken of the finished lug to ensure the cutting procedure had not induced any delamination. The final lug specimens, as typified in Figure 28, were found to be void-free.

Lug Element Tests - Room temperature testing was performed with a load rate of 500 lbs/sec, and all lugs were tested in as received moisture condition. The testing setup is shown in Figure 29. In order to keep the gap between the lug and loading clevis surface at 0.1", which was used in the analytical models, special bushings were fabricated. A different gap size might cause unexpected failure loads due to different pin bending effects.

The lugs with 1.75" diameter holes (W/D = 2.0) exhibited a catastrophic fiber failure at the net section, whereas the lugs with 1.0" diameter holes (W/D = 3.5) showed permanent yielding around the hole prior to shear/bearing failure. The initial bearing failure load was determined by observing the behavior of axial strain data from rosettes located at 0.5" away from the edge of the 1.0" hole and 0.25" away from the 1.75" hole at the center line of specimens. Load versus strain data indicates that axial strain decreases with associated material failure ahead of the pin for the 1.0" hole lugs, Figure 30. Typical failed specimens are shown in Figure 31. These results for the six lug configurations are summarized in Figure 32 along with analytical predictions.

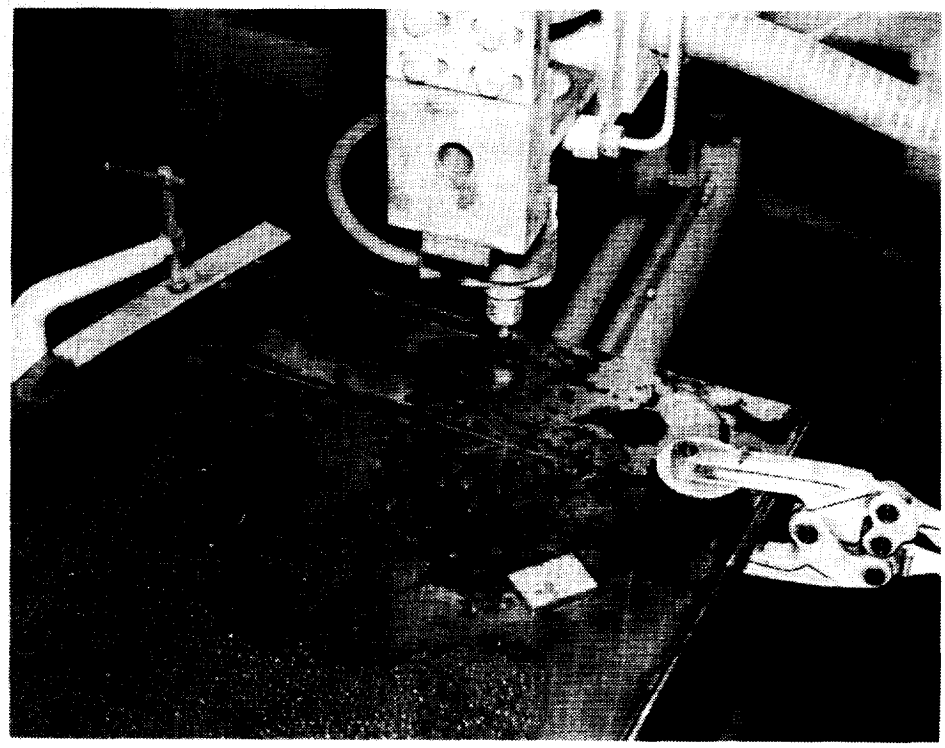

Figure 27 Thick Composite Lug Elements were Efficiently Machined Using Abrasive Waterjet Cutting

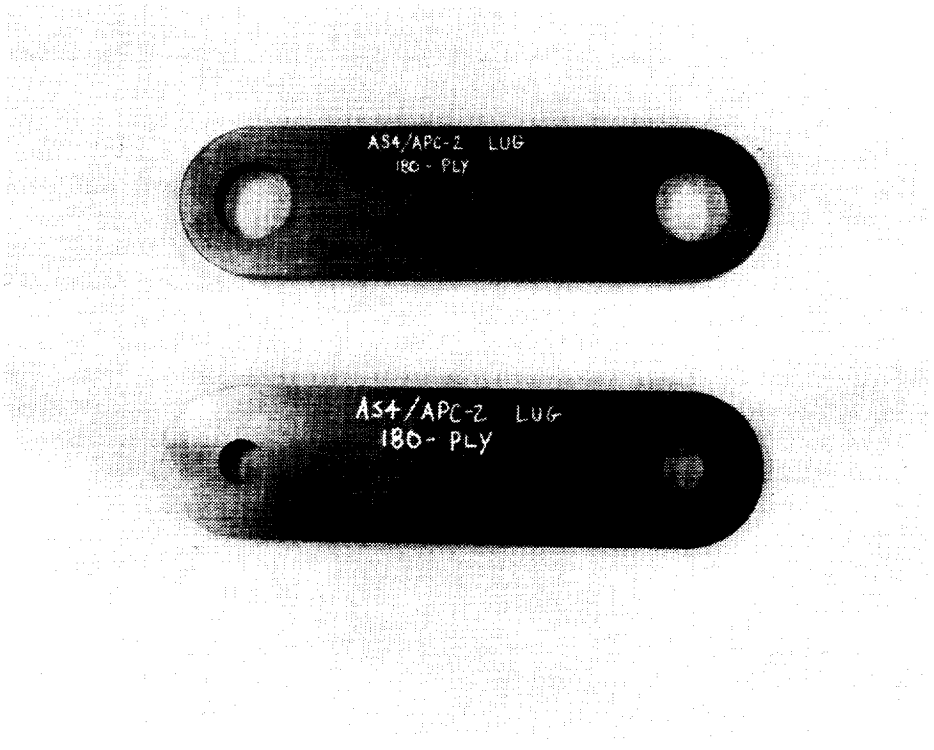

Figure 28 Two W/D Geometries were Used to Demonstrate Distinctly Different Failure Modes

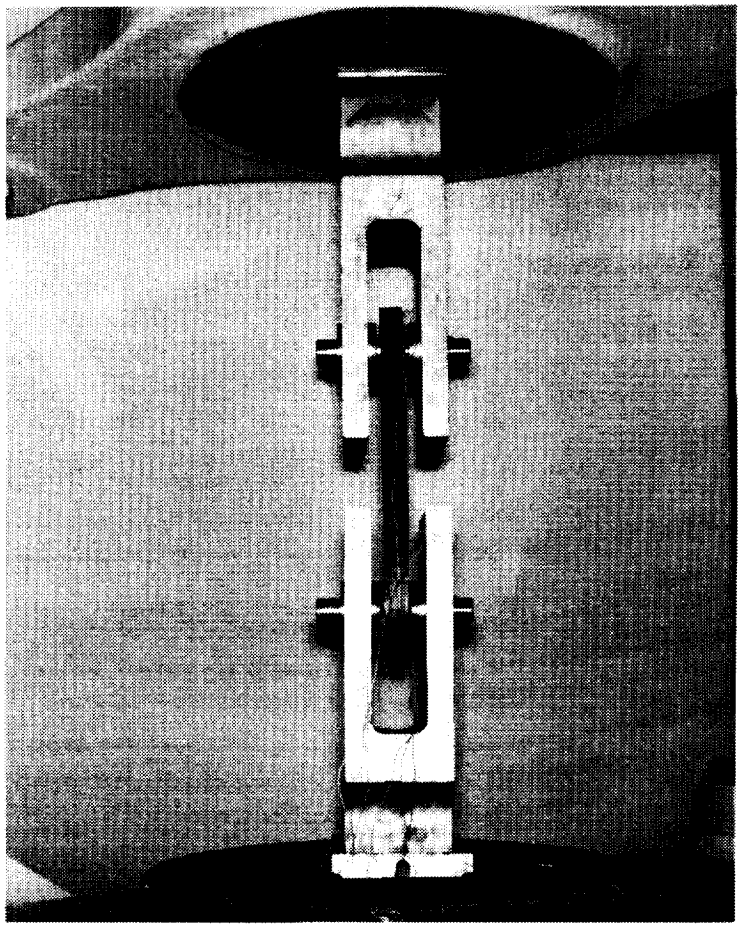

Figure 29 Lug Element Test Set-Up Simulated In-Plane Loading

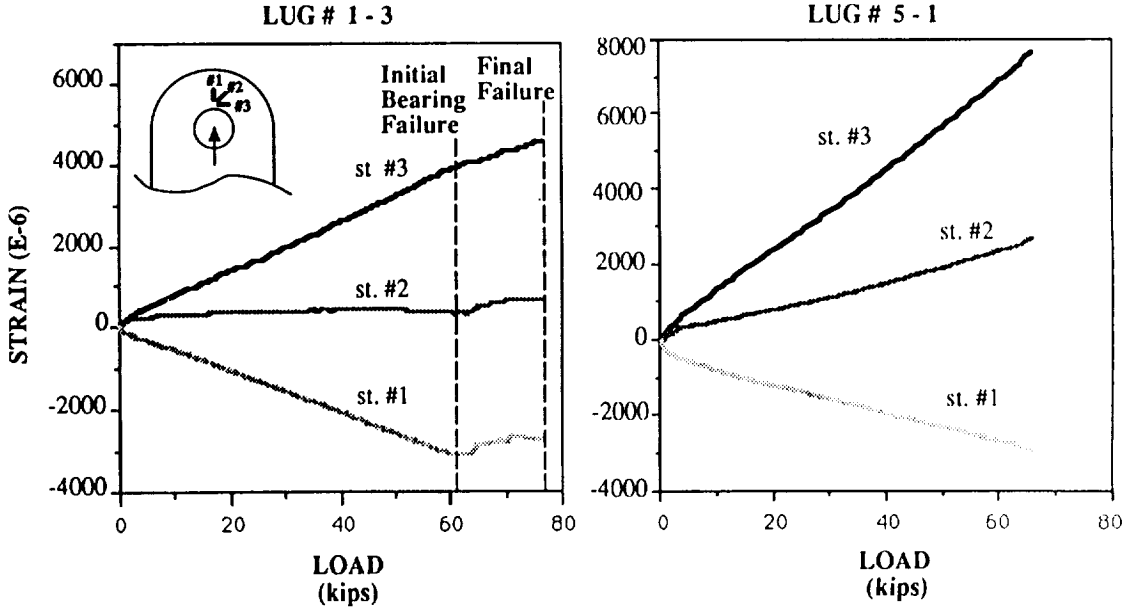

Figure 30 Lug Element Load vs Strain Data Provided Accurate Determination Of Failure

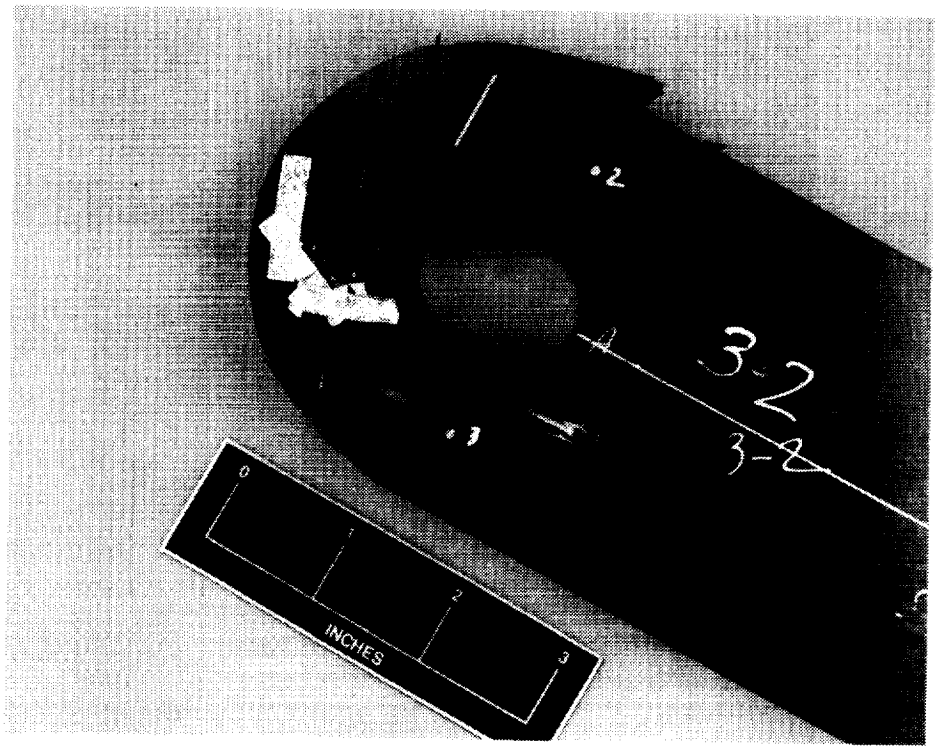

Bearing and Shear-Out Failure Observed for 1.0" Diameter Lugs

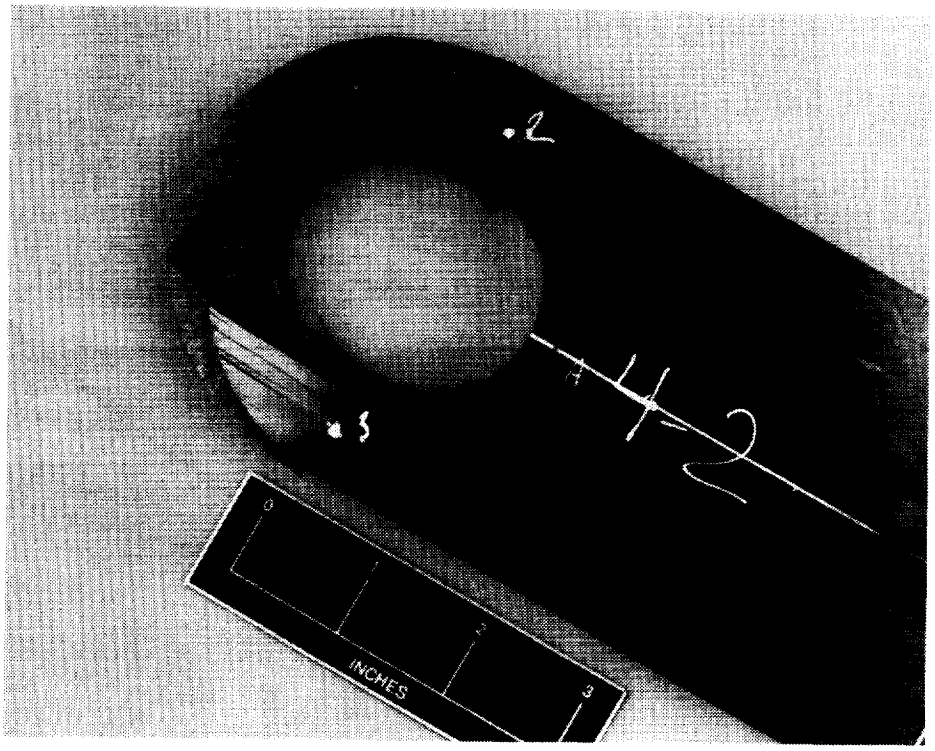

Net-Section Failure Observed for 1.75" Diameter Lugs

Figure 31 A Range of Lug Element Failure Modes were Demonstrated

Lug Specimen	Quantity Each	Hole Dia. (in)	Pred. Failure Load (kips)	Average Test Results (kips)	Standard Deviation
#1	4	1.0	64.2	60.1 (76.7)*	4.3 (2.2)
#2	3	1.0	65.9	62.3 (74.3)*	6.9 (3.0)
#3	4	1.0	57.3	62.2 (74.7)*	7.0 (2.0)
#4	4	1.75	66.9	69.3**	3.1
#5	4	1.75	66.5	68.7**	2.9
#6	4	1.75	61.5	66.8**	1.8

* Initial Bearing Failure Load (Final Failure Load)

** Failure Load

Figure 32 Close Agreement Between Predicted and Actual Lug Element Strengths was Achieved

Rolled Formed Stiffeners

Vanguard Composites Company (Anaheim, CA) was subcontracted to fabricate 45 feet of roll formed hat stiffeners. These stiffeners were to be originally used in subcomponent fabrication using the fiber placement process, but served as a manufacturing demonstration due to the redirection.

The thermoplastic hat stiffener consisted of 7 plies of IM7/ITX which incorporates a 4 ply drop-off in the flanges representative of the fiberplaced panel design. A single layer of 3 mil neat PEEK film is incorporated on the IML of the flanges for future bonding trails. C-scans of the first article hat stiffener showed a lack of consolidation in the flange ply drop-off area as well as in the stiffener walls in the area of the upper radius. The first article also had visible roller lines transverse to the stiffener's length and dry patches on the IML flanges where the neat resin film had thinned out.

A second article showed slightly better consolidation in the ply drop-off areas but still had poor consolidation in the stiffener walls. The roller marks were eliminated and the neat resin film application looked much better on the second article. It was discovered by Vanguard that the roller for consolidation of the stiffener walls had a 1/2° mismatch which was most likely the reason for the inadequate consolidation in this area. The problem was corrected and fabrication continued.

Forty-five feet of roll formed hat stiffeners was received from Vanguard Composites Company. A typical section is shown in Figure 33. NDT results from a random sample of the hat stiffeners show a lack of adequate consolidation in the flange area. The constant thickness portion of the flanges showed significantly better consolidation. Based on these observations, it is felt that roll forming of constant cross-section, thermoplastic composite stiffeners with uniform flanges is a viable manufacturing process. However, tapered flanged stiffener concepts would require additional development.

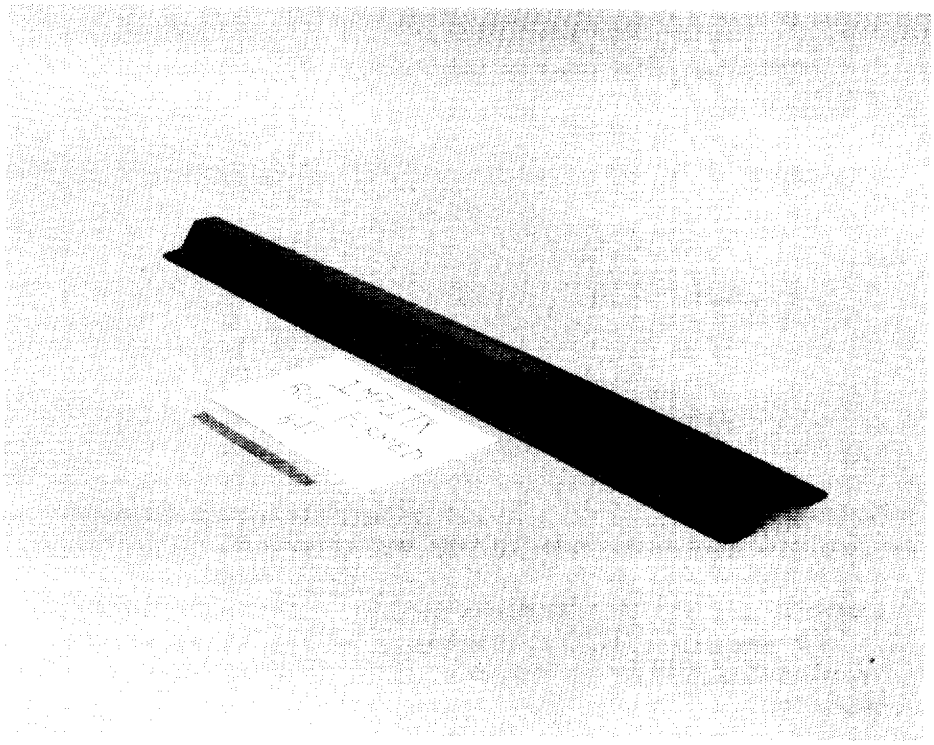

Figure 33 Rolled-Formed Hat-Section Stiffeners Demonstrated Potential for Low Cost Manufacturing

CONCLUSIONS AND RECOMMENDATIONS

Thermoplastic composite development pursued in this program, while directed toward fighter aircraft structure, is equally applicable to commercial vehicle structure. These developments focused on critical composite issues associated with primary fuselage structure, fastenerless moldline, upper fuel cell cover structure, and thick lugs representative of those on carry-through bulkheads. Activities by a D/MI team were carried out in the areas of structural mechanics, manufacturing concepts development, and structural validation. A summary of element design, fabrication, and structural testing was presented in this report.

Elemental manufacturing verification trials produced valuable lessons learned. In the SDCC Y-frame activities simple tooling modifications such as blended stiffener mandrel and pressure box ramp intersections coupled with aluminum diaphragms eliminated diaphragm ruptures. Polymeric diaphragms are still desirable from a cost point of view, but as yet do not have the necessary elongation properties needed for complex forming.

A one-step SDCC process was a program goal, however, ply dragging/ wrinkling problems necessitated going to a two-step process which yielded production quality parts. While the two-step process provides cost savings over conventional three-step diaphragm forming, the one-step technique should still receive industry attention since additional cost savings could be realized.

The development of a positive drive tooling concept for the blade frame elements came about as a need to correct inadequate intersection consolidation pressure inherent in the original tooling. The addition of selected keyways to the tooling allowed for segmented tooling details to be directed (positively driven) during pressure application resulting in a first-time quality part. In addition, a previously rejected blade element was reconsolidated to production quality in the modified tooling demonstrating the potential cost savings associated with the ability to reconsolidate thermoplastic composites.

Roll-forming may be a viable technique for producing long, relatively constant cross-section stiffeners. While sections produced in this effort did not reach production quality consolidation, overall cross-section geometrical tolerances, straightness in length, and repeatability were quite good. Investigations in this program revealed that while there is still some development necessary, this approach should receive additional industry attention.

Thick laminates (1.0 inch) were manufactured to production quality by consolidating a series of sublaminates. An additional benefit of this effort was the demonstration of abrasive water jet cutting as an effective means of machining thick composites. Edge surface finish was found to be very acceptable for high tolerance areas requiring only modest surface reaming or finishing for low tolerance areas.

Significant pull-off strength increases were demonstrated in the Y-frame concepts compared to conventional blade design. Testing of the fastenerless frame concepts has provided the necessary experience with these designs to allow for risk reduction in future scale-up to subcomponent and full-scale structure.

REFERENCES

1. Hoffman, P. L. R. and Gibler, J. A., "Design for Manufacturing, Producibility Issues for Thermoplastic Composites," presented at SAMPE Spring Meeting, Anaheim, CA, April 4, 1990.

2. Renieri, M. P., Burpo, S. J., and Roundy, L. M., "Design and Manufacturing Concepts for Thermoplastic Structures," First NASA Advanced Composites Technology Conference, Seattle, WA, November 1990, NASA Conference Publication 3104.